Institutionen för naturgeografi
och kvartärgeologi

Stockholms universitet

# The potential of Synthetic Aperture Radar for the monitoring of small scale slushflows and slush avalanches in the Atigun Pass, Alaska

Katreen Wikström

Examensarbete grundnivå
Geografi, 15 hp

GG 47
2012

# Preface

This Bachelor's thesis is Katreen Wikström's degree project in Geography, at the Department of Physical Geography and Quaternary Geology, Stockholm University. The Bachelor's thesis comprises 15 HECs (a half term of full-time studies).

Supervisor has been Ian Brown at the Department of Physical Geography and Quaternary Geology, Stockholm University. Examiner has been Peter Jansson, at the Department of Physical Geography and Quaternary Geology, Stockholm University.

The author is responsible for the contents of this thesis.

Stockholm, 26 January 2012

Lars-Ove Westerberg
Director of studies

Cover Picture: A truck approaching the Atigun Pass (Photo by author)

# ABSTRACT

The scientific field of remote sensing is constantly developing as the image quality improves and the demand increases when new research topics evolve. For many years snow scientists have used microwave synthetic aperture radar (SAR) imagery to map different types of snowcovers, however few have related their studies to avalanche forecasting. The aim of this study is to implement the technique of SAR imagery over the central Brooks Range in Alaska, United States, to investigate the potential in monitoring of slushflows and slush avalanches. The site is well-known for being a dangerous traverse during the winter, because of the high avalanche danger. Also in the snowmelt season, the steep mountain slopes are prone to avalanches of significantly higher water content. Fine beam, C-band, HH-polarized SAR images from the RADARSAT-1 satellite were available for this study. An analysis of temporal backscatter variation and a change detection analysis of return signal brightness in the images were performed in ENVI. So, what did the results finally show? With a resolution of 6.25 m, SAR is still too course to catch small-scale slushflows and slush avalanches. The technique is useful for larger-scale wet snow mapping, which by interaction with topography may contribute to useful material for risk zoning of slush snow. The study demonstrates many of the issues that still remain within remote sensing and the most important is the geometry aspect; the impact of the satellite sensor's incidence angle on radar backscatter, especially when working with high relief terrain, and the subsequent radiometric distortions due to this factor, which delimit the information content of the imagery. The study further illuminates the importance of using high resolution digital elevation models for terrain correction, as if not, images taken from different passes (ascending or descending orbits) cannot be stacked together in the change detection analysis. Different snow properties also have an effect on the radar backscatter coefficient, which has been tested in the study. Air temperature data appears to be helpful for the comprehension of the backscatter values, where small warming events or sudden temperature drops have a significant impact on the radar return signal. Despite difficulties with SAR, the study establishes the idea of using specific radar backscatter values of slush snow in avalanche forecasting, to map larger scale risk zones for slush avalanches and slush flows.

# TABLE OF CONTENT

## LIST OF FIGURES



## LIST OF TABLES

# 1. INTRODUCTION

In the Atigun Pass in the central Brooks Range, Alaska, slushflows and slush avalanches occur each year during the snowmelt period (Onesti, 1987). Slushflows and slush avalanches are snow avalanches that contain a large amount of liquid water, which makes them very dense and able to transport large debris volumes down the slopes (e.g. Nyberg and Rapp, 1998 and Jaedicke et al, 2008) at a speed of up to 60 m $s^{-1}$ (Hestnes and Sandersen, 2000). Slushflows and slush avalanches are typical for high latitude alpine regions and they get released each year, due to the very sudden and strong solar input after the long and persistent winters (Onesti, 1985), but can also get released in the mid-winter due to rain events (Eckerstorfer and Christiansen, 2010). They have been reported all over the northern hemisphere in sub-arctic and arctic regions, e.g. on Svalbard (Eckerstorfer and Christiansen, 2010), Iceland (Decaulne and Saemundsson, 2006), Sweden (Nyberg and Rapp, 1998) and Norway (Hestnes, 1998). The cold and shallow snowpack, that is typical for these northern latitudes, becomes quickly saturated with water when it rains or the sun heats the snow surface, which results in slabs, or flows of slushy snow, to start slide downhill (Onesti, 1985).

For studying snowmelt processes at remotely located arctic and sub-arctic sites, microwave remote sensing has become a useful tool. In optical imagery, one cannot differentiate between dry and wet snow, but in centimetre length microwave data, the dielectric properties of dry and wet snow are different (Fily et al, 1995). Thus, wet snow mapping is already an established application of microwave remote sensing (e.g. Baghadi et al, 2000, Nagler and Rott, 2000, Dean et al, 2006). Change detection analysis of avalanche snow was performed by Sharma et al (2004) in the Himalayas by using multi-temporal optical and active microwave imagery. However, any wet snow mapping has not yet been achieved for the central Brooks Range region in Alaska. The motive of this study is to further investigate the potential of synthetic aperture radar (SAR) within this particular field. Here we employ change detection of eight RADARSAT-1 SAR images over this particual area from the snowmelt period of May and June in 2005 and 2007, and we use a dry winter referance image from January. To understand the complex snowpack at the Atigun Pass, field work was conducted from the first week of May 2011. Air temperature data from 2007-2011 have been used to develop a comprehensive illustration of the snowmelt period at the study site. Atigun Pass is a good test location for slushflow and slush avalanche detection, but the area is poorly covered by high resolution SAR images. Hence, this study shows at the difficulties and the limitations that still exist today within remote sensing of small-scale features in alpine, remote areas, using active microwave sensors.

## 1.1 Aim of study

Mapping of wet snow by using SAR imagery is an established practice, though not in relation to slushflows and slush avalanches. The aim of this study is therefore to study the potential of SAR imagery for wet snow mapping in relation to the monitoring of such hill slope movements.

# 2. THEORETICAL BACKGROUND

The theoretical background of microwave remote sensing is complex and most often described in terms of physical concepts and mathematical models. The following theory chapter has the purpose of presenting the basics of the physics behind microwave remote sensing, which is important to understand the processing of data, the results and the discussion of this paper. The basic concepts of surface- and volume scattering are here described and equations are used to show how various parameters impact on the scattering mechanisms.

## 2.1 Microwave remote sensing of snow

SAR images have unique capabilities that lead to a wide range of applications. SAR typically operates at centimeter wavelengths and can therefore penetrate through clouds and even dry snow layers on the ground (Woodhouse, 2006). A synthetic aperture radar transmitts pulses of radar waves towards the area of interest on the ground and records the energy intensity (or backscatter) of the signal that returns to the antenna (Woodhouse, 2006). The transmitted pulses reach the ground at different depths, depending on their specific radar signal (so-called band, which are of different wavelengths) and at different incidence angles, depending on the sensor's beam mode and the slope angle of the terrain. When studying snow, C-band is most often used because of its suitable radar frequency of 5.3 GHz and a wavelength of 5.7 cm (ESA, 2011a). C-band can penetrate through the upper soil-layer and through dry snow up to 20 m (Martinez-Vazquez et al, 2005). SAR typically operates at given polarizations, normally co-polarized vertical or horizontal. The preferred type of polarization depends on the geometric structure of the target that is studied (ESA, 2011b). As snowpacks most commonly are structured with horizontal layers, the most suitable polarization for many snow studies is HH, which means that the radar wave is both transmitted and received horizontally (ESA, 2011a).

The spatial resolution and the all-weather operating capabilities of SAR have contributed to an important progress in the mapping of high relief terrain (e.g. Shi and Dozier, 1995, Partington, 1998, Nagler and Rott, 2000). Although, SARs do have limitations; the geometric distortions in radar images can be significant. Steep mountain slopes are the most problematic topography to work with, as layover effects and radar shadow areas frequently appear due to the side-looking geometry of the imaging radar antenna (Fig 1) (Woodhouse, 2006).

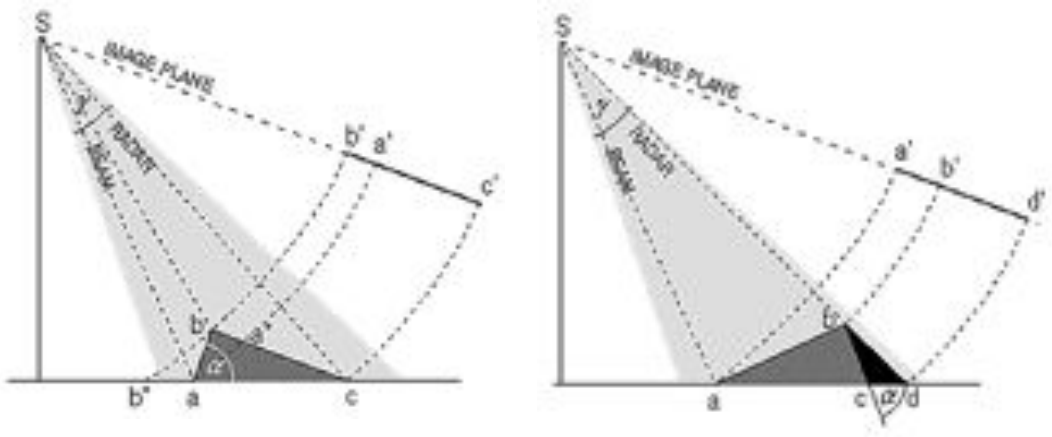


*Fig 1. Geometric distortions; lay-over (left) versus radar shadow (right) effects (Images clipped from Fig 1.8 Geometric distortions, ESA, 2011b)*

## 2.2 Surface- and volume scattering

The intensity of the radar return signal is often rescaled to decibel values to give the average scattering cross section per unit area, also called backscattering coefficient, $\sigma_t$. (Guneriussen, 1997). The relative dielectric constant, $\varepsilon_r$, of the medium that is studied and satellite sensor parameters such as geometry, frequency and polarization, all impact on the total backscattering received. Guneriussen (1997) showed that the local incidence angle has a large impact on the backscattering coefficient. The backscattering coefficient of the radar wave may give us information on whether the ground is snow-covered or not, as well as the characteristics of the snowpack. Dry and wet snow backscatter very differently. When the radar wave intercepts the dry smooth snow surface, part of it gets reflected immediately while the rest penetrates into the snow and gets refracted or absorbed (Fig 2) (ESA, 2011b).

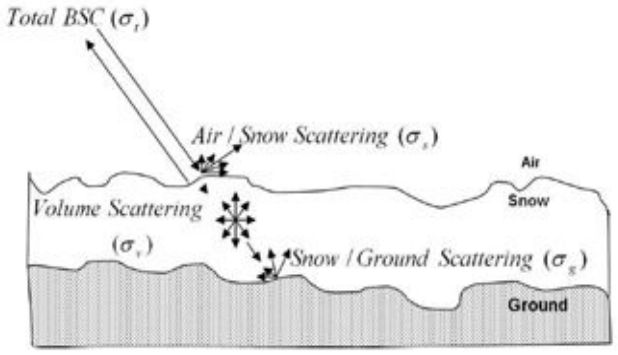


*Fig 2. Mirowave interaction with snow-covered terrain exhibiting surface, volume and snow/ground interface scattering phenomena (from Singh and Venkataraman, 2010)*

An electromagnetic wave propagates through a medium depending on its dielectric constant. The complex dielectric constant of a medium, $\varepsilon_r$, is the sum of the permittivity, $\varepsilon'$, minus the imaginary dielectric loss, $\varepsilon''$, i.e. the energy that the medium absorbs; conventionally written as (Rees, 2001)

$$\varepsilon_r = \varepsilon' - i\varepsilon'' \qquad \text{(Eq. 1)}$$

An instrument working in C-band (5.3 GHz) such as RADARSAT-1, has the radar wavelength of 5.7 cm. Because of the large penetration depth of dry snow, a shallow dry snowpack becomes largely transparent in SAR data (Baghdadi et al, 1998). The high dielectric loss of wet snow increases the absorption coefficient and drastically reduces the penetration depth to only a few centimeters as soon as a very small percentage of liquid water is present in the snowpack (Shi and Dozier, 1995). According to Rott and Nagler (1993) the penetration depth of snow with 1% liquid water is 13.8 cm while with 3% liquid water it gets reduced to only 4.9 cm. In snow mapping, the varying backscatter signal is used as the main component in the separation of wet and dry snow (Dean et al, 2006).

The total backscattering from a medium is the sum of surface-, volume and ground (i.e. surface) scattering (Fig 2 and 3). These two different forms of scattering are here going to be explained, by using models from Rees (2001) and Guneriussen (1997).

Wet snow is dominated by surface scattering, $\sigma_{0ss}$, due in part to the shallow penetration of the microwaves. Surface scattering is here modeled by using the so-called Kirchoff's stationary phase approximation (Ulaby et al, 1982 from Rees, 2001);

$$\sigma_{0ss}(\theta) = \frac{|\Gamma(0)|^2 \exp[-\tan^2 \theta / 2m^2]}{2m^2 \cos^4 \theta}$$

(Eq. 2)

where Γ is the Fresnel's reflection coefficient for non-magnetic media and $m$ is the root-mean-square surface slope, which is $\sqrt{2}\,(\Delta h/L)$ where $\Delta h$ is vertical roughness and $L$ is the correlation length (Rees, 2001). The absolute $|\,\Gamma(\theta)\,|^2$ part of this model shows that the reflection coefficient is a function of the incidence angle.

The other type scattering, volume scattering, $\sigma_{0sv}$, can be explained by the following model, which combines the so-called Born approximation and Rayleigh's scattering (from Guneriussen, 1997);

$$\sigma_{0sv}(\theta) = \frac{24\pi^4 r^3 v \cos(\theta')}{\lambda^4 \kappa} |K|^2 \left(1 - \frac{1}{L^2(\theta')}\right)$$

(Eq. 3)

where;

$$|K| = \left| \frac{\varepsilon - \varepsilon_0}{\varepsilon + 2\varepsilon_0} \right|$$

(Eq. 4)

and θ' is the incidence angle, $r$ is the radius of spherical scatters in volume, $v$ is the volume fraction of ice, $\varkappa$ is the extinction coefficient and $L$ (θ') is exp( $\varkappa d$ sec θ'), which is the one way propagation loss in the snowpack and $d$ is snow layer thickness (Guneriussen, 1997). However, as pointed out earlier, when modeling the actual backscattering of a snowcover, wet or dry, one must combine the volume scattering with surface- and ground (surface) scattering, which can be done in a simple way. The total backscatter for a dry snowcover can be calculated by $\sigma_{dry} = \sigma_{0ss} + \Gamma(0)^2\,(\sigma_{0sv} + \sigma_{0sg} + L^{-2})$ and for a wet snowcover by $\sigma_{wet} = \sigma_{0ss} + \Gamma(0)^2\,(\sigma_{0sv} + L^{-2})$ as we neglect the snow-ground interface because of the high dielectric loss within the wet medium (Guneriussen, 1997).

Regarding the backscattering signal, previous studies by Dean et al (2006) showed that an increase of the liquid water content in the snowpack leads to a decrease in total received backscatter, but also that when the snow surface becomes more and more wet during snowmelt, it becomes rough which results in a varied surface scatter (Fig 3).

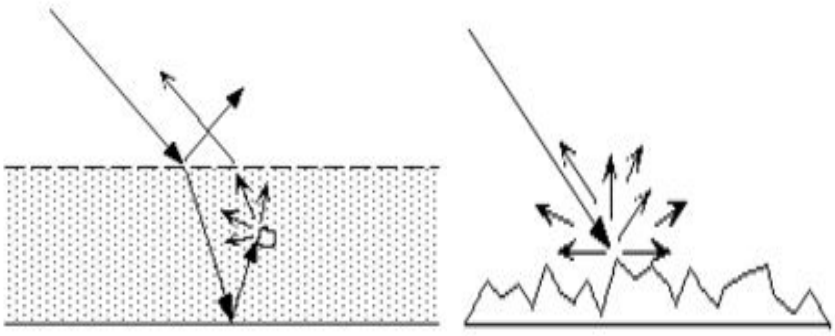

*Fig 3. Volumetric (left) versus rough surface scattering (Images clipped from Fig 1.7, ESA (2), 2011)*

Magagi and Bernier (2003) demonstrated the relationship between the measuring instrument's incidence angle, due to specific beam mode, and the scattering that it results in. They used RADARSAT-1 SAR data from the S7 beam mode with an incidence angle of 45-49° and the S1 beam mode with an incidence angle of 20-27°. The higher incidence angle resulted in dominating volume scattering of the total signal and the lower incidence angle resulted in dominating surface scattering. Thus, their study further emphasizes the function of the incidence angle in the equations listed above.

## 2.3 Radar backscatter of wet snow

The typical returning power signal of wet snow is usually -14 dB (Shi and Dozier, 1995) which is about 3 dB lower than for dry snow (Koskinen et al, 1997). However, Magagi and Bernier (2003) found only a 1 dB threshold between wet and dry snow when working with RADARSAT-1 C-band data. Hence, a conventional dB value for wet snow is still a topic of research. Snowpacks backscatter differently depending on the stage of snowmelt (e.g. Dean et al, 2006; Magagi and Bernier, 2002). Investigations have shown that a wet snowpack with a liquid water content > 4% (very wet) leads to a rough snow surface and therefore a dominating surface backscattering. Hence, the backscatter coefficient increases throughout the snowmelt (Dean et al, 2006, Magagi and Bernier, 2002). However, in the study by Dean et al (2006), it was also shown that a moderately wet snowpack (1-3% liquid water) generates lower backscatter values than a dry snowpack. In the literature, the backscattering relationship between dry, wet and very wet snow is well-described; e.g. Shi and Dozier (1995) found a positive correlation between surface roughness and backscatter for very wet snow and a negative correlation for a smooth surface.

# 3. SLUSH AVALANCHES AND SLUSHFLOWS

Slush avalanches and slushflows are hill slope mass movements that are typical for arctic and sub-arctic alpine environments. A slush avalanche is defined as a "slab release of water-saturated snow" (Fredston and Fesler, 1999). It is important to differentiate between wet and slush avalanches. In the literature, classifications have been made depending on their magnitude and liquid water content. Nyberg and Rapp (1998) graded these hillslope movements in order of slush avalanches, slushflows and slush torrents. By their classification, the snowpack is water-saturated in prior to slush avalanche release, of even higher water content for slushflows , which also travel faster downhill (Fig 4) and the slush torrents are the most infrequent movements but of highest water content. However, all these types of wet snow mass movements have geomorphic impacts in the high latitude alpine environment as transformers of the landscape by erosion and debris transport (Nyberg and Rapp, 1998). Their highly destructive impact has been explained by their relatively high velocity (up to 60 m $s^{-1}$) which is due to their high snow density which causes a low internal friction of the snow grains (Jaedicke et al, 2008).

Slush avalanches and slushflows can occur on gentle slopes; the starting zone ranging from 15-20°, although the lower slope can be of much lower angle (Tremper, 2008). In the northern hemisphere, they usually occur on south-facing slopes in troughs of steep chutes or in gullies, but also in smaller basins in valleys (Fig 5). This is where snow accumulates most and is protected from being removed by wind, but where they are exposed to direct sunlight for many hours during the day (Onesti, 1985). The dynamics of slushflows and slush avalanches are still a matter of concern, as field data from the starting zones are very difficult and dangerous to get. Although, e.g. Bozhinskiy and Nazarov (1998) and Gauer (2004) have presented models describing their dynamics (Jaedicke et al, 2008).

*Fig 4. Slushflow in motion, 3 June 1995, Kärkevagge, northern Sweden (Nyberg and Rapp, 1998)*

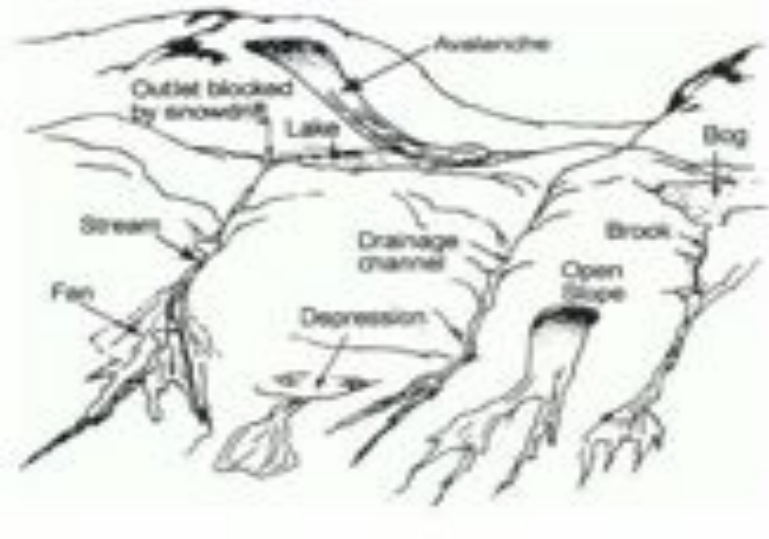


*Fig 5. Starting zones of slushflows (Hestnes, 1998)*

The required meteorological conditions for slushflows and slush avalanches have been well-reported. Cold, persistent winters followed by a very rapid snowmelt, caused by the strong solar input during spring, that is typical for these latitudes, contribute to their release (Onesti, 1985). Often at these latitudes, the snowmelt period lasts for only one month, not uncommonly with solar irradiance of 24 hours per day (Scherer et al, 1998). Slushflows and slush avalanches can also be caused by individual rain events that suddenly increase the liquid water content of the snowpack (Jaedicke et al, 2008). With the fast thawing, the snowpack becomes quickly isothermal; the entire snowpack has a temperature above 0°C (Onesti, 1987). In high latitude environments the snowpack often lies on impermeable permafrost soil which prevents water percolation (Tremper, 2008). Also ice-crust layers within the snowpack can prevent further percolation and hence contribute to a concentration of liquid water in the upper layer of the snow profile (Fig 12).

When the liquid water content increases within the snow, the mechanical bonding (so-called shear strength) between the snow grains reduces (Onesti, 1987). Wet snow reaches different stages of saturation depending on the level of liquid water content (Colbeck, 1975). In these different stages, or regimes as Colbeck (1975) call them (Fig 6) the pendular regime is the early stage and implies that the ice grains are still exposed to air, while at a higher water saturation the ice grains become surrounded by water, that leads to rapid loss of shear strength. This might also explain why two snow layers of different densities (i.e. liquid water content) slide so easily on top of each other, especially snow on top of an ice-crust (Colbeck, 1975).

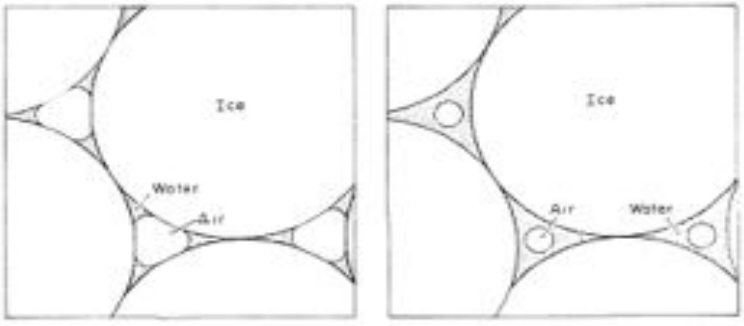


*Fig 6. Pendular (left) versus funicular (right) saturation regimes of snow grains (Colbeck, 1975)*

# 4. STUDY AREA

The Atigun Pass is located at 68°08' N 148°29' W along the Dalton Highway in the central Brooks Range, Alaska (Fig 7). It is the highest (1444 m above sea level) and the most northern highway pass in the state. In the winter months the Atigun Pass is exposed to many avalanches which make it a risk area for people crossing the pass (O'harra, 2001).


*Fig 7. Location of the Atigun Pass. Image processed by author, based on Aster DEM (Alaska Mapped, 2011)*

During the snowmelt period in spring, many slopes in the central Brooks Range are prone to slushflows and slush avalanches (Onesti, 1985, 1987). Onesti observed by his investigations in the 1980's that the slushflows in the central Brooks Range usually occur from the third week of May to the first week of June, when the air temperatures start to rise and even daily minimum temperatures are above freezing (Onesti, 1985). The melting period is usually very intense, as the snow can be almost gone in a week from the day when the melting starts. According to Walker et al (1999) the intense snowmelt period is typical for arctic snowpacks. As demonstrated in Fig 8, the air temperatures in May the last five years have shown a similar behavior as discussed by Onesti. A significant rise of the air temperatures around the 20-25$^{th}$ of May may be the start-off to the slushflow and sluh avalanche period, even though the air temperatures may decrease, but most often continue on a steadily increase for the rest of the snowmelt period. Further, starting around the third week of May, the gap between minimum and maximum temperatures per day suddenly increases (Fig 9). Such temperature peaks may lead to that the snowpack becomes isothermal the same day (Table 1).

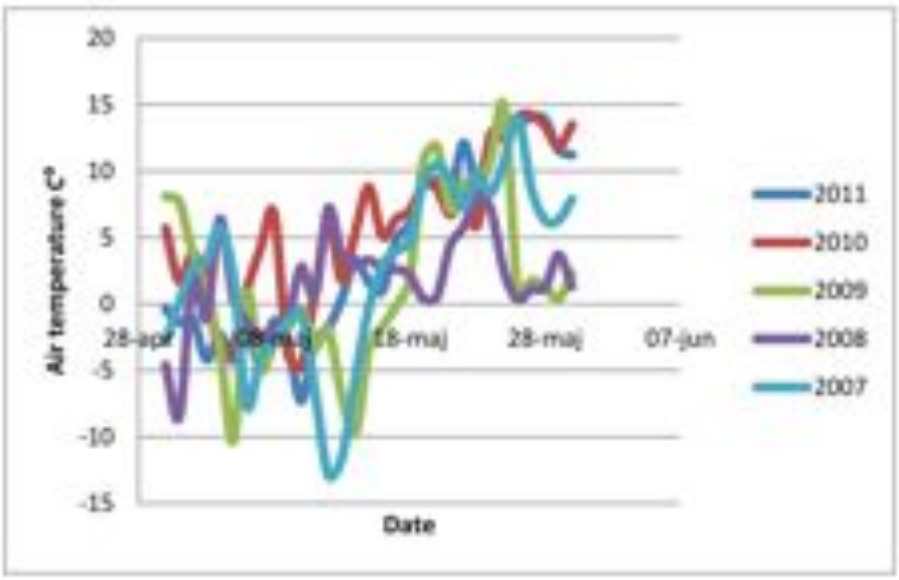


*Fig 8. Daily maximum temperatures measured at the Atigun Pass weather station, May 2007-2011 (Chart based on data from NRCS, 2011)*

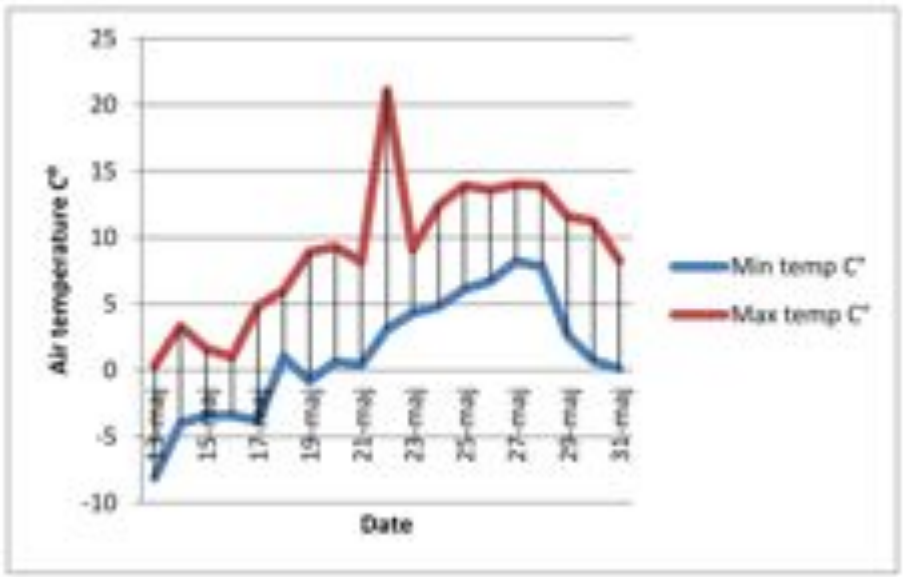


*Fig 9. Daily minimum and maximum air temperatures at the Atigun Pass weather station, May 13-31, 2011 (Chart based on data from NRCS, 2011)*

**Table 1. Snowpack temperatures at location B2, 8th of May 2011 (description of location in chapter 5.4)**

| Depth (cm) | 1:00 PM | 4:50 PM |
|---|---|---|
| 1 | -5.3 | 0.2 |
| 20 | -2.4 | 0.1 |
| 40 | 0 | 0.1 |
| 60 | 0.1 | 0.1 |
| 80 | 0.1 | 0.1 |
| 100 | 0.1 | 0.1 |
| 120 | N/A | N/A |

With a clear sky and solar radiation all day, the snowpack temperatures increase drastically and the snowpack may become isothermal by mid afternoon (see Table 1) even though the average air temperatures are below zero. On the other hand, a spread of wet patches on the snow (Fig 11) does not necessarily mean that slushflows and slush avalanches must be approaching within a couple of days. The next morning, they may all be refrozen again, as melt- and refreeze cycles are common during the spring months.

The following photos present the characteristics of the Atigun Pass which makes it a typical slush-prone area; the topography of wind-blown ridges and gullies with accumulated snow (Fig 10) and the dynamics of the snowcovers that last until far into the snowmelt season (Fig 11-12). They are all important components to include in this spatial analysis.

*Fig 10. Gullies with accumulated snow and wind-blown ridges (Photo by author)*

*Fig 11. Patches of wet snow (Photo by author)*

*Fig 12. Ice-crust layers in a gully witnessing melt-refreeze cycles (Photo by author)*

# 5. METHODOLOGY

## 5.1 Processing of data

Synthetic Aperture Radar images from the RADARSAT-1 satellite have been used previously in avalanche forecasting for extraction of wet snow (e.g. Sharma et al, 2004). Eight RADARSAT-1 images were used for this study; all were C-band products of the fine beam mode and of HH-polarization, taken from an incidence angle of 37-38°. Four images had the acquistion year of 2005; the reference image from January 9th and snowmelt images from May 1st, 25th and June 18th, and four images from 2007; with the reference image from January 23rd and snowmelt images from May 23rd, June 8th and 16th. Jan 9th and May 25th from 2005 and Jan 23rd, May 23rd and June 16th from 2007 were all images taken from a descending orbit, whereas May 1stand May 25th from 2005 and June 8th of 2007 were from an ascending orbit.

At first, digital elevation model tiles from the 30 m ASTER Global Digital Elevation Map were mosaiced to provide a terrain model for geometric correction. After that, the SAR images were processed in MapREADY, a SAR processing software developed by the Alaska Satellite Facility. In MapREADY the digital values were converted to backscatter coefficients, i.e. the radiometry was selected to sigma nought with output scale in decibels. Then radiometric terrain correction was applied with the DEM mosaic to reduce radiometric distortions in the images, where resolution was fixed to 6.25 m. At last geocoding was applied to the UTM map projection for zone 6 and datum WGS84.

## 5.2 Image analysis

After the image pre-processing in MapREADY, the resampled images were further processed and analyzed in the remote sensing software ENVI (Environment Visualizing Images). The image analysis was conducted by following steps (1) delimit geographical area; (2) perform speckle filtering; (3) plot four terrain option areas to gain backscatter values over time; and last (4) implement a change detection analysis by using the Band Math tool.

The demarcation of the geographical area to focus on, was made with consideration to cover both slush prone gullies, non slush prone slopes as well as the road winding over the Atigun Pass. The final delimited window covered an area of 343 samples and 317 lines.

The purpose of speckle filtering is to decrease the anomalous variability (speckle) in the images, to improve the information content of the imagery (Woodhouse, 2006). However, speckle filtering affects the spatial resolution of the images, as pixels are being homogenized. The application of any speckle filtering in ENVI converts the dB values to values in an 8-bit, 0-255 greyscale. Most common in SAR processing, is to rescale the raw SAR data to dB values as the last step, but here it was done during the pre-processing in MapReady. It is not possible to rescale back to dB values once speckle filtering has been performed. By taking the maximum and minimum RGB values in the images divided by the maximum and minimum dB values in the original images, a linear scale of equivalent 8-bit – dB values was achieved (see attached document). This scale was used later on for analysis of the backscattered values in the filtered images. One must merge reduction of speckle noise with the ability of preserving edges and textures, i.e. contrast, in the image when evaluating speckle filters (Xiao et al, 2003). After testing different speckle filters and sizes, the adaptive enhanced lee filter with filter size of 3x3 pixels was chosen, the small size was adopted because of the small-scale features that are studied for which high spatial resolution is important. The chosen speckle filter succeeded best to homogenize areas and at the same time preserve edges and texture information in the images.

Plots with backscatter values associated with four different terrain options areas

were produced for 2005's and 2007's snowmelt period. TO1 and TO2 represent slush prone areas, at the Atigun Pass expected in the gully, therefore presented as "Gully lower" and "Gully upper" in the plot (Fig 13). TO3 and TO2 represent "non-prone slush areas", in the diagram marked as "Wind-blown slope" (lack of snow) and "Road". Four pixels with the exact same geographical location, no matter year of acquisition, were chosen by linking together the eight images. The TO locations were chosen thanks to terrain observations in May 2011, but also with regard to geometrically induced radar distortions. No pixels with values lower than -19 dB were used, in order to not exceed the sensor's sensitivity level of -22 dB.

The last step in ENVI was to perform a change detection analysis by using the Band Math tool. In this processing, the initial stage (reference image) is subtracted from a final stage (snowmelt image) to illustrate any change in brightness between two stages. Performing Band Math does stretch out the values once more to new 8-bit values which makes it not possible to use the dB scale that was associated with the original unfiltered images.

### 5.3 Air temperature data

The National Resources Conservation Service has maintained a weather station at the Atigun Pass since 1999. Their SNOTEL sensors monitor a wide range of climatic parameters, e.g. air temperature, solar radiation, wind speed, snow depth etc. The historical weather archive of the Atigun Pass weather station is unfortunately paltry. Neither solar radiation nor soil moisture data has been reported earlier than August 2007, data that naturally would have been very helpful for a snow mapping analysis. Nevertheless, average daily air temperatures from 2007 had been reported and irregularly taken air temperature measurements from 2005, which were used in this study.

### 5.4 Field measurements at study site

The objective of the field work conducted at the Atigun Pass in May 6-11$^{th}$ (2011) was to get an idea of the spatial topographical variation and snowpack characteristics. However, as the SAR images cover a much larger area, the focus in field was set on understanding the important processes more in detail at a couple of chosen locations. Snowpits were excavated at three sites. At each site a different number of snowpits were excavated, depending on its relevance for the study.

Way-points were taken with a GPS and notes of acquisition time, slope aspect (taken with a compass), slope angle (taken with a clinometer), cloudiness, precipitation and wind (observations) were written down. A digital camera was used to take photos of snow profiles and certain features that were of interest. Snow temperatures were measured throughout the profiles with a thermometer on a 20 cm interval. The stratigraphy of the snowpack and other surrounding features were observed.

An investigative focus was put on a gully, named location B, located on the left-hand side of the road just south of the Pass. Two days of field measurements were conducted here in order to record temporal change in the snowpack due to varied weather conditions during the week of field work. Snow depth, snow temperature, stratigraphy and density were measured on four spots of different altitude along the gully (B1:1 – B2:1). At location B1:1 and B2:1 snow temperatures were measured twice a day.

The image processing products and air temperature data of the SAR acquisition period are reported in the following Results section.

# 6. RESULTS

The aim of this chapter is to present the results achieved from processing and analyzing the SAR images in ENVI, along with a presentation of the air temperature data over the same period of time.

## 6.1 Analysis of temporal backscatter variation

Four different terrain types were represented by localized study sites. Called "terrain option areas" these were chosen as to present two typical slush prone and two non slush prone sites, located nearby the Atigun Pass. Fig. 13 shows the locations of the four terrain option areas and their geographical locations area listed below the figure.


*Fig 13. Specific locations of TO areas; (left) input of image subset (January 23, 2007) into extract of the Atigun Pass area from Google Earth and; (right) TO locations 1-4 in SAR image (January 23, 2007)*

TO1; Lower gully (68°6'58.28" N 149°32'54.12"W)
TO2; Upper gully (68°7'17.05"N 149°32.56.20" W)
TO3; Wind-blown slope (68°7'11.09" N 149°32'27.99" W
TO4; Road (68°7'2.64 N 149°32'43.02" W)

The backscatter intensity at each location was sampled for each of the time intervals per image. The results of the temporal backscatter variation analysis are presented in Table 2.

There is no doubt that, at first glance, the results look dramatically different for the two different snowmelt periods. The backscatter values from the reference images were in accordance for the two years in the expected slush-prone areas; in the lower gully -11.5 dB for Jan 9 (2005) and -12 for Jan 23 (2007), as the accuracy is about 2 dB. In the upper gully the backscatter values were -5.8 dB and -6.6 dB respectively. But for the non-slush-prone areas, the values differed more; at the wind-blown slope with -7.4 dB for January 9 (2005) and -11.8 dB for January 23 (2007) and -16.6 dB and -13.4 dB received at the road. However, the backscatter values were of considerably greater variance during the snowmelt period.

**Table 2. Radar backscatter values of four terrain types (TO 1-4) from 2005 and 2007. TO1 represents the lower gully, TO2 the upper gully, TO3 is the location for a wind-blown slope and TO4 is the road. The backscatter values were received in the 8-bit greyscale unit and were converted linearly to decibel values.**

| Terrain option | 2005 | 8-bit greyscale | Decibel | 2007 | 8-bit greyscale2 | Decibel |
|---|---|---|---|---|---|---|
| TO1; | January 9 | 188 | -11.5 | January 23 | 186 | -12 |
| Gully lower | May 1 | 167 | -17.2 | May 23 | 202 | -7.7 |
| | May 25 | 168 | -16.9 | June 8 | 228 | -0.7 |
| | June 18 | 191 | -10.7 | June 16 | 185 | -12.3 |
| | | | | | | |
| TO2; | January 9 | 209 | -5.8 | January 23 | 206 | -6.6 |
| Gully upper | May 1 | 181 | -13.4 | May 23 | 205 | -6.9 |
| | May 25 | 190 | -11 | June 8 | 174 | -15.3 |
| | June 18 | 182 | -13.1 | June 16 | 227 | -0.9 |
| | | | | | | |
| TO3; | January 9 | 203 | -7.4 | January 23 | 187 | -11.8 |
| Wind-blown | May 1 | 203 | -7.4 | May 23 | 195 | -9.6 |
| slope | May 25 | 171 | -16.1 | June 8 | 179 | -14 |
| | June 18 | 210 | -5.5 | June 16 | 185 | -12.3 |
| | | | | | | |
| TO4; | January 9 | 169 | -16.6 | January 23 | 181 | -13.4 |
| Road | May 1 | 198 | -8.8 | May 23 | 194 | -9.9 |
| | May 25 | 161 | -18.8 | June 8 | 169 | -16.6 |
| | June 18 | 164 | -18 | June 16 | 161 | -18.8 |

In 2007, the lower (TO1) and upper (TO2) part of the gully backscattered similarly on May 23rd, but differed greatly by June 8th. The varying values on June 8th could probably be explained by a changed wetness in the snowpack; with a damped snow surface in the lower, flat part of the gully which may have generated high surface scattering, while the upper, steep, part of the gully was just wet which generated typical wet snow backscattering. Also at the non slush prone locations, backscatter values influenced by wetness seem to have appeared, as on May 23rd both the wind-blown slope and the road backscattered right below -10 dB and then by June 8th the backscattering were values associated to wet snow.

To further illustrate the distinction of the two snowmelt periods, brightness change between several stages has been detected in the following Change detection analysis

## 6.2 Change detection analysis

The results of the change detection analysis are presented in Fig. 16. The backscatter values in Fig. 16 and in Table 2 are presented in 8-bit digital number values, since they could not be converted to decibel as they were once again stretched out to a new 0-255 scale when they were analyzed in ENVI. Due to the weak results of the terrain correction in MapREADY, the images that were taken from an ascending orbit, could not be used with any of the references images as both reference images were from a descending orbit. These circumstances applied to May 1st (2005), June 18th (2005) and June 8th (2007); of which the last image was completely excluded from the analysis once this condition was detected.

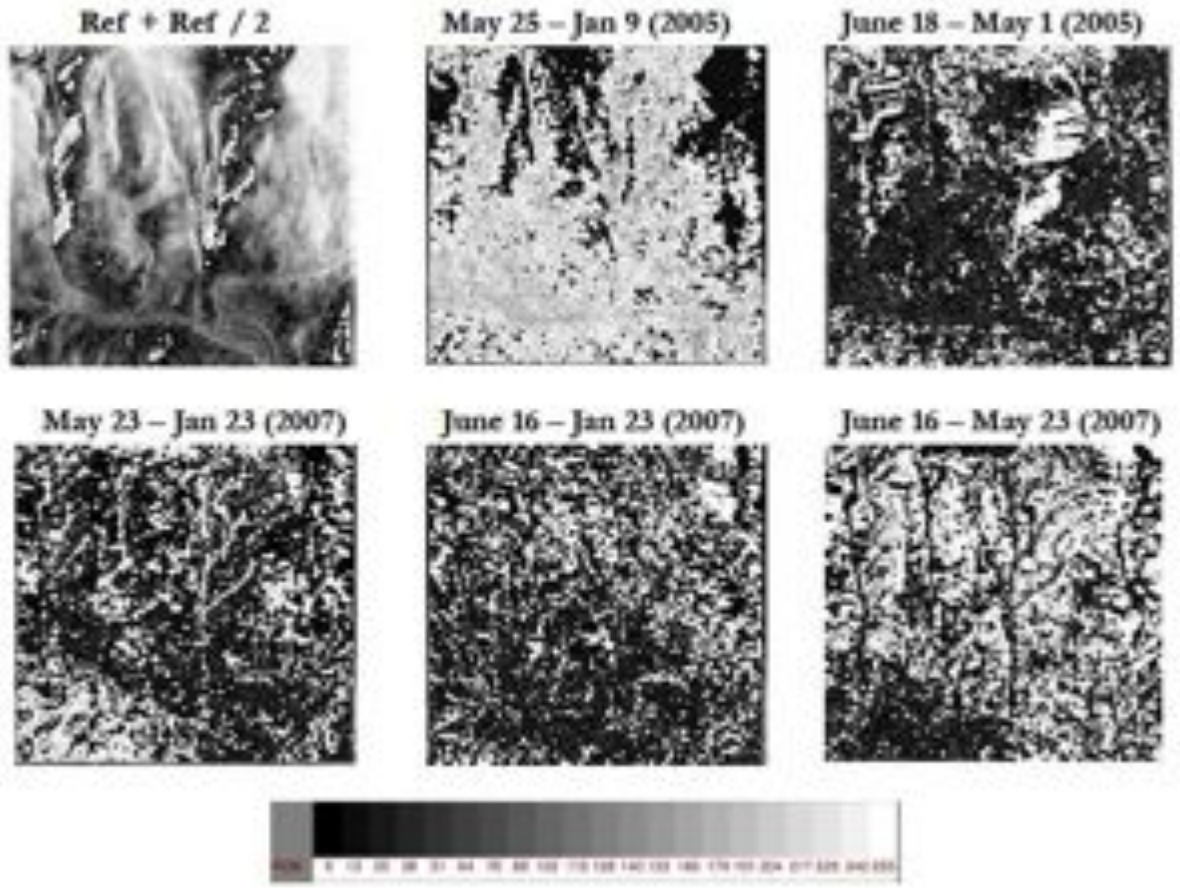


*Fig 14. The results of the change detection analysis. Final stage – initial stage was performed in Band math. (Top left) image demonstrates the difference in backscatter that is even between two dry snow images; here January 9 (2005) that was added with January 23rd and then divided by two, which resulted in small areas of brightness change. (Top middle) image shows brightness difference in May 25th comparing to reference image. Due to the lack of a reference image with an ascending orbit, the two ascending snowmelt images were subtracted from each other, shown in the (top right) image. For 2007 there were two snowmelt images with a descending orbit, and the reference image was subtracted from both of them; the results are shown in (bottom left) image and (bottom middle) image. The (bottom right) image shows the brightness change between the previous two.*

A visualization of the snowmelt period of 2005 was not possible to achieve, due to the geometric factor explained above. The (top right) image in the figure, should still be as applicable as the resulting (bottom right) image, which shows the brightness change between May 23rd and June 16th (2007). This conclusion was drawn after the following example; if a pixel in the reference image has a value of 100, a pixel in image 1 has a value of 50 and a pixel in image 2 has a value of 150 and the final – initial stage is performed; the resulting image 1 pixel receives a value of -50 and the image 2 pixel a value of 50. If then the initial stage (image 1 pixel) is subtracted from the final stage (image 2 pixel) the final result is 100. Further, if the same procedure is performed but excluded the first step with the reference image, the final result will still become 100, as 150 – 50 = 100.

For 2007 there were two images representing the snowmelt period that were taken from a descending orbit. This resulted in a snowmelt dataset with higher information content. As we can see visually in Fig. 16 for the (bottom left) and (bottom middle) images, there were more absorption of the radar signal taking place at June 16th than at May 23rd, i.e. larger areas of wet snow, but there are also areas of increased brightness in the two

images. Increased brightness does not necessarily indicate that the surface was covered with dry snow; high backscatter may also indicate bare ground that is exposed in a broken snowcover (see radar backscatter description in the Theoretical background chapter).

**Table 3. (a; top) Single band backscatter values before change detection; mean and standard deviation values and (b; bottom) mean- and standard deviation values after change detection, for each of the images shown in Fig. 14**

| | Mean (greyscale) value | Stdev (greyscale) |
|---|---|---|
| **2005** | | |
| January 9 | 181.6 | 35.6 |
| May 1 | 169 | 35.9 |
| May 25 | 158.9 | 55.1 |
| June 18 | 180.5 | 32.2 |
| **2007** | | |
| January 23 | 184 | 34.3 |
| May 23 | 189 | 32.7 |
| June 8 | 154.4 | 51.6 |
| June 16 | 190.2 | 31 |

| | Mean (greyscale) value | Stdev (greyscale) |
|---|---|---|
| (Jan 9 - Jan 23)/2 | 129,5 | 72,1 |
| **2005** | | |
| May 25 - Jan 9 | 163,6 | 96,4 |
| June 18 - May 1 | 86,2 | 101,9 |
| **2007** | | |
| May 23 - Jan 23 | 92,8 | 109 |
| June 16 - Jan 23 | 90,9 | 109 |
| June 16 - May 23 | 126,9 | 115,2 |

The statistics presented in Table 3a and b might be perceived as a bit misleading. However, the mean values shown in the Table 3a are mean backscatter values of an image, whereas Table 3b shows mean values of brightness *change* between two images. The mean value here does not represent what happened on a smaller scale, which is the emphasis of this paper, referring to small scale slushflows and slush avalanches. To detect brightness change of these, we study particular features in the image, e.g. the gully. The gully can be picked out in Fig 14. *d* as it appears brighter by May 23rd than in January 23rd, though it disappears among other wet and bright areas in the June 16th image. The gully is also the location for the two slush-prone areas, and the *f* image demonstrates an increased wetness through the snowmelt period; comparing its snowcover from May 23rd to June 16th. On the other hand, if the brightness change is due to a radiometric factor or actual snow wetness change is hard to determine with the few images available. Another aspect to regard as well is the possibility that the gully may have gone through several cycles of melt and re-freeze in between the two dates of SAR acquisition, and what is displayed in the final image (*f*) is a result of that process. However, the areas that are brighter in this image, are probably so because they are now exposed ground and not covered by dry snow anymore, since they were wet already by May 23rd. As explained in the Theoretical background chapter, bare rock and dry snow backscatter similarly.

## 6.3 Air temperatures

Air temperatures have been measured by the SNOTEL sensor located at the Atigun Pass and data from its historical archive was used in this study. Air temperature charts of May – June 2005 and 2007 based on the NRCS data are shown in Fig. 17 and 18. However, the chart of 2005 was incomplete as measurements were taken irregularly. Important to emphasize here is that the charts represent *average* daily air temperatures. One must remember that the night (minimum) temperature may have been far below freezing and the afternoon (maximum) temperature may have been far above freezing (Fig. 9). As air temperatures can fluctuate greatly throughout the day during the snowmelt period, the average air temperatures presented here only give us a very generalized picture of the snowmelt period. Unfortunately, neither minimum nor maximum daily air temperatures were reported in the NRCS's historical archive.


*Fig 15. Average air temperatures in May-June 2005. Due to irregular measurements, the chart cannot show any trend besides the individual daily temperatures (Chart based on data from NRCS, 2011)*

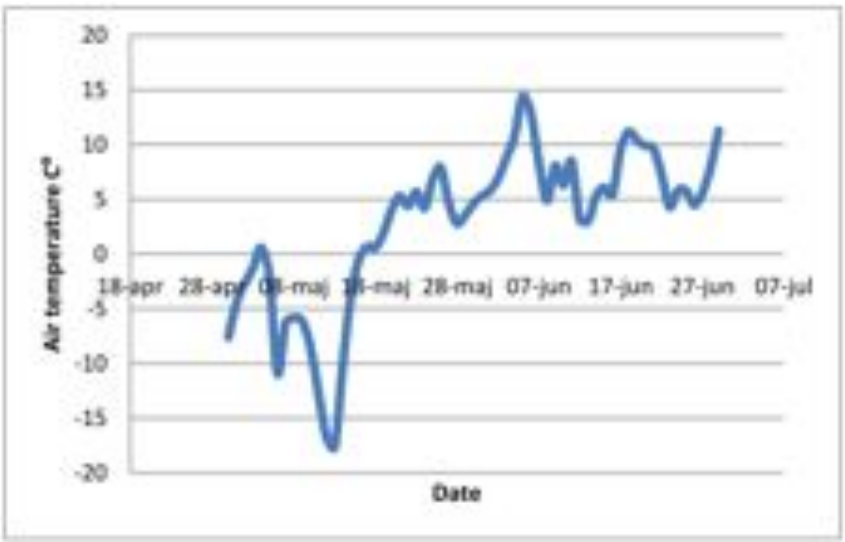


*Fig 16. Average air temperatures in May-June 2005 (Chart based on data from NRCS, 2011)*

The air temperatures of 2007 follow the general May-June trend for the Atigun Pass (Fig. 8), with a sudden air temperature peak around the third week of May and thereafter a steady continued rise including occasional temperature drops, though not below freezing. The May-June air temperatures from 2005 on the other hand, were not in accordance to the trend of air temperatures that is shown in Fig. 8, comparing it to Fig. 17. Very fluctuating air temperatures throughout the entire month of May, followed by warm temperatures by the beginning of June and at last a sharp temperature drop down to almost freezing by mid/end of June makes the air temperature period of 2005 an exception. Since the objective of using air temperature data is to enhance the comprehension of the SAR imagery results, the inadequate measurements of year 2005 does not fully meet the objective.

# 7. DISCUSSION

In this chapter the methodology applied and results achieved in this study are discussed, along with a critical analysis of SAR and its limitations, Atigun Pass as a study site and the relevance of using SAR imagery as a tool for monitoring of slushflows and slush avalanches at this particular study site.

The central Brooks Range in Alaska, is often mentioned as a locale for slush avalanches and slushflows in the avalanche literature (e.g. Tremper, 2008) and became well-covered by Onesti (1985, 1987)describing their formation and meteorological conditions in prior to release. However, in the literature, no mapping of slush avalanches and slushflows, or even wet snow, have been done since, for this particular area. Nevertheless, discrimination of wet snow by using SAR data has been performed in other parts of the world (e.g. Baghdadi et al, 2000, Nagler and Rott, 2000, Strozzi et al, 1999). As mentioned in the introductory chapter, Sharma et al (2004) performed a change detection analysis of radar backscattering values from an active microwave sensor to monitor snow avalanches in the Himalayas. Based on this, there must be reasons for why snow scientists have not investigated this topic further. This leads us to establish the following research questions:
What is the potential of SAR imagery in the monitoring of slushflows and slush avalanches?
What are the limitations of the technique?
And, in the terms of this study: What could have been done differently?

## 7.1 Data processing and image analysis

There are many ways of processing and analyzing SAR data and the methodology chosen for this study is just one of many ways. The SAR image coverage over Alaska is fairly poor which directly reduces the options of alternative methods. Furthermore, the available SAR imagery is provided by the Alaska Satellite Facility who recommends processing the data in their own program MapREADY. Working with remotely sensed imagery is both time-consuming and filled with risks for error due to the method you choose to apply. If time and resources were different, it would have been interesting to compare the processing results from MapREADY with other manual processing methods. Terrain correction was performed with a mosaic of tiles derived from the 30 m ASTER Global Digital Elevation Model. It would be interesting to see if the resulting resampled images would have been different if the images were terrain corrected with a higher resolution digital elevation model. This should, for example, improve the accuracy of the radiometric terrain correction.

The topography of the Brooks Range is very steep which in SAR imagery generates layover effects and shadowed areas. Images from when the satellite took both ascending

and descending orbits were used in this case. Desirable though would have been to have images of exactly the same acquisition dates to stack together and thereby possibly delimit the effects due to the sensor's geometry. When analyzing the data in ENVI it is here important to only interpret values that are above the sensor's sensitivity level. As slushflows and slush avalanches usually are associated with gullies where the accumulation of snow is high and also stays deep until late in the season (Onesti, 1985), we face another problem as these gullies most often happen to be in these "no value areas", i.e. shadowed or layovered. The gully that was put into focus in this study seems to be able to represent varying backscatter independently.

The complexity of topography may have a large impact on the snow mapping results from the SAR images. The slope's aspect, orientation and gradient may influence the properties of the snow and the radiation balance at that certain slope (Dean et al, 2006). Radiometric distortions increase significantly in high relief terrain since the backscatter is in part dependent on the incidence angle (Fig. 1). In radar shadows the sensor does not receive any direct return signal. For slopes that are facing directly towards the sensor, the effect is opposite; they become very bright and lower backscatter values become difficult to distinguish. To cope with the problem of radiometric distortions, satellite images taken with a higher incidence angle are desired. By using images from a sensor of higher incidence angle than 38°, the radiometric distortions may have been less extent in this study, as referring to Sharma et al (2004) who used images taken with incidence angles of 39-44° for their study in the steep Himalayan mountains, as reflectivity decreases with an increased incidence angle (ESA, 2011a).

Another method to apply when working with high relief terrain is to use images taken from both ascending and descending orbits. This is as a matter dependent on the availability on suitable data, a fact that had an important impact on the outcome of this study. Due to the lack of a reference image taken from an ascending orbit, it was not possible to produce a visual scheme over the snowmelt period of 2005. Often, terrain correction with a high resolution digital elevation model can solve the problem of various orbits. Critique towards the performance of the digital elevation model that was used for terrain correction in this study is therefore relevant. It is important to once again stress, since the results of this study demonstrate the issue, the digital elevation model is crucial for whether the SAR images will be able to contribute to any useful information.

## 7.2 Spatial and temporal backscatter patterns

The results attained in Table 2 present the radar backscatter coefficient of four different terrain option areas, four pixels, of which two were expected to be slush-prone; the upper and the lower part of a gully, and two were expected to be non-slush-prone; a wind-blown slope and the road. The selection of these four sites was based on observations in field in May 2011 and with accordance to GPS way-points. Also taken into consideration, was to choose pixels that were within or close to the dry and wet snow value range. The results showed on very different backscatter values, which of course was expected. However, the pixel values represent an average of an area of 6.25 x 6.25 m which means that within that particular area, several terrain features may be present. Slushflows and slush avalanches may be small in size.

The road backscattered quite similarly in both years, with a low reference image value (January 9$^{th}$ -16.6 dB and January 23$^{rd}$ -13.4 dB), followed by a snowmelt period in May-June with initially high values (-8.8 dB and -9.9 dB respectively) and much lower towards the end (around -18 dB for both years).

In the upper gully we have a reference image value of -5.8 dB and -6.6 dB respectively. In 2005 a value of -13.4 dB on May 1$^{st}$ followed by a value of -11 dB for May 25$^{th}$. As mentioned earlier, the "normal" snowmelt period would probably appear as the

contrary. By studying the April air temperatures of 2005, which are not presented in any graph in this paper, there was a small warming event by the end of April and afterwards average air temperatures stayed below freezing until the end of May. Although, the measurements were irregular so it is not possible to say if that was exactly what happened, but it could testify to the anomaly that we witness. On the other hand, air temperatures above freezing before the third week of May is not an anomaly in itself; rain events throughout the winter can cause the snowpack to become isothermal and release into slushflows and slush avalanches much earlier than the annual snowmelt period (Eckerstorfer and Christiansen, 2010). For all that, the May air temperatures in 2007 are more in accordance to the temperature trend shown in Fig 8. The backscatter values from the upper gully also demonstrate this more "normal" behavior of a snowmelt season, with more expected values. At May 23rd we get a value of -6.9 dB, followed by -15.3 dB at June 8th and up to -0.9 dB by June 16th. The actual air temperature for these dates were 4.4°C at May 23rd, 8.4°C at June 8th and 6.1°C at June 16th. Although, here we can imagine the snowpack in the upper gully to be largely affected by the temperature peak right before June 8th, which maybe have caused the snow surface to become very wet by the day of SAR acquisition (June 8th) which also maybe lead to widespread snowmelt that resulted in a very sparse snowcover by June 16th. If that was the case, that would further explain the very high (bright) radar backscatter of that particular day.

In the lower gully, we have a much lower reference image value (-11.5 dB in 2005 and -12 dB in 2007), which might be partly due to a higher incidence angle. Moreover, the two snowmelt periods look very unlikely between the two years. In 2005 we get a May 1st value of -17.2 dB, which as for the upper gully, could be explained by an early warming event that took place by the end of April (which is not shown in Fig. 16 (NRCS, 2011)). For May 25th the value stayed low, -16.9 dB, but rose to -10.7 dB by June 18th. Probably the low backscatter values represent a wet snowcover which by the brighter condition at June 18th supports this suggestion, as the snow most likely was gone by then. For 2007, the lower gully has a value of -7.7 dB by May 23rd, a rise up to -0.7 dB by June 8th and then a fall down to -12.3 dB by June 16th. As pointed out already in the Results chapter, the high value on June 8th in the lower gully, comparing to a value of -15.3 dB from the upper gully, could possibly be explained by an extremely wet and rough snow surface that lead to surface scattering, i.e. high (bright) backscatter values. The sudden temperature peak right before this day, shown in Fig 16, and then continuing above-freezing temperatures further supports this argument.

In this discussion, we cannot avoid to discuss once more the impact of slope angle on SAR geometry. The upper and the lower part of the gully look peculiarly different to each other. The upper part is step and narrow, while the lower part is wide and flat. The disperse terrain of the two could definitely explain the distinct backscatter values acquired at the same day. In the analysis of the temporal backscatter variation, the theory of ascending versus descending passes and their impact on backscatter was tested, to assure that no simple assumptions of low backscatter equals wet snow and high backscatter equals dry snow or bare rock were made without consideration of other impacts involved. According to the theory of incidence angle and the impact on radar backscatter, different backscatter values may appear due to ascending and descending passes. The theory would explain why one with images from an ascending pass, could get higher backscatter values on a steep slope than on a flat slope; as the steep slope faces directly towards the sensor. However, this theory did not agree with the results of this study. In the images taken from an ascending orbit, the values were higher from the flat slope than from the steep slope for two of three images. And in the images taken from a descending orbit, the flat slope gave lower values than the steep slope for all of the three images, which would have been the opposite according to the theory, since the steep slope would have been in the shadow area

and thereby could have generated lower backscatter. The incidence angle can have an important impact on the backscatter, but the results of the temporal variation analysis in this study rather show on wetness differences between the upper and lower gully, than direct effects of different incidence angles.

A wide variation in backscatter values, although the actual snow conditions were known, may be explained by the fact that there is no apparent correlation between liquid water content of the snow and observed backscatter. As Dean et al (2006) observed in northern Sweden, higher backscatter values were received in some of the wet snow images than in the dry snow images. However, higher backscatter values may appear when the ground has been frozen. Also, they observed that the variation of backscatter values become more considerable later during the snowmelt as the snow gets a rougher surface which leads to surface scattering instead of volume scattering. Late during the snowmelt when there are only patches of snow left, i.e. a broken snow cover, the areal backscatter average in the satellite images may also be from exposed ground in between the snow patches. Hence, the geophysical and dielectric properties of snow are usually more consistent earlier in the winter when the snowpack is dry. Therefore, it is important to consider the diurnal melt and re-freeze of snow surfaces, upon which may have had a major impact on what is shown in the SAR imagery. The backscatter coefficient is therefore depending on what specific hour during the day the imagery was taken and the stage of stratification in the snowpack (Dean et al, 2006).

## 7.3 Snowcover modeling

Snowpacks are extremely dynamic and change appearance each year, even throughout the season and from one day to the other. Hence it is recommended to analyze SAR imagery that have the same acquisition dates as the executed field work and the same resolution scale as the targets of study. For this study, unfortunately none of these prerequisites were completed. The satellite images were from 2005 and 2007 and can thereby only represent the snowmelt period of those particular years. RADARSATs FN1 mode that provided the images for this study has a resolution of 6.25 m which might be too coarse for small-scale slushflows and slush avalanches.

Ground-truth data is necessary for modeling of the backscattering coefficients of a snowpack at a particular study site (Magagi and Bernier, 2002). Field measurements of snow water equivalent are essential for the forecasting of snowmelt runoff, and other field parameters such as snow depth, density, liquid water content and stratification are important to be able to evaluate a snowpack (Fily et al, 1995). Snow parameters as those listed by Fily et al (1995) began to be measured in August 2007 at the Atigun Pass, which makes this study lacking some important snow parameters. Field measurements handed out in May 2011 were used to describe the study site. They were not of such an extent that they could have been used for any statistics or as parameters in the backscatter models.

However, to cope with the problems of lacking ground-truth data, we can use values for snow properties from the literature. The models for surface- and volume scattering that were presented in the Theoretical chapter were here implemented by using the incidence angle of 38°, which was valid for the SAR images in this study, snow densities of 300-500 kg $m^{-3}$ (Onesti, 1987), numbers for root mean square surface slope of delta H = 0.009-0.017m and L = 0.150-0.24 m based on the study by Barber and LeDrew (1994) and values for dielectric permittivity (1.4-2.6) and dielectric loss (0.00058-0.9) (Guneriussen, 1997) based on values of liquid water content for dry, wet and slush snow from the International Classification of Seasonal Snow on the Ground (Colbeck et al, 1990). The total backscatter for a dry snowcover can be calculated by $\sigma_{dry} = \sigma_{0ss} + \Gamma(0)^2 (\sigma_{0sv} + \sigma_{0sg} + L^{-2})$ and for a wet snowcover by $\sigma_{wet} = \sigma_{0ss} + \Gamma(0)^2 (\sigma_{0sv} + L^{-2})$ (Guneriussen, 1997). To model the ground scattering, the parameters $\varepsilon' = 5$ and $m = 0.5$ from Guneriussen

(1997) were used and put into the surface scattering model. By using these variables, that are also listed in Table 4, the total backscattering for different snow covers were modeled. The models generated a backscatter coefficient of -4.2 dB for very dry snow (0-1% water), -14.0 dB for wet snow (3-8% water) and -16.3 dB for slush (> 10% water). The results correspond adequately to the backscatter coefficients achieved in similar models that have been implemented for dry and wet snowcovers (e.g. Shi and Dozier, 1995).

**Table 4. Dielectric properties and geometric variables used in the volume-, surface- and ground scattering models**

| Medium | | Wv | r | v | ε' | ε'' | m | Γ(0) | | |
|---|---|---|---|---|---|---|---|---|---|---|
| *Dry* | | 0-1% | 0.00033 | 0.32715 | 1.4 | 0.0005 | 0.5 | -0.20893 | | |
| *Wet* | | 3-8% | 0.001 | 0.43621 | 2 | 0.15 | 1.3 | -0.30712 | | |
| *Slush* | | >10% | 0.005 | 0.54526 | 2.6 | 0.9 | 2 | -0.37281 | | |
| | | | | | | | | | | |
| **Medium** | | **εsnow** | **εair** | **L** | **Θ** | **d** | **Lp** | **σ** | | **dB** |
| *Dry* | | 0.422577 | 0.663225 | 2.56 | 38 | 2 | 21.27956 | 0.381561 | | *-4.19* |
| *Wet* | | 0.353553 | 0.663225 | 1.8 | 38 | 2 | 0.08478 | 0.039616 | | *-14.02* |
| *Slush* | | 0.310087 | 0.663225 | 1.36 | 38 | 2 | 0.016111 | 0.024821 | | *-16.31* |

The modeling in Table 4 shows that backscatter values below -16 dB are likely to indicate the presence of slush. Values greater than -5 dB indicate strong backscatter from the ground surface, suggesting dry snow or an absence of snow. The typical backscattering of a dry, wet and slush snowcover may be used for guidance in the interpretation of the backscatter values shown in Table 2. Although some backscatter values lower than -16 dB were present even at the non-slush-prone locations, they are more relevant to analyze for the slush-prone locations, as the topography and the snow depths at these sites increase the risk for slushflows and slush avalanches. Values below -16 dB were for example found at May 1st and 25th (2005) in the lower gully. The wind-blown slope also indicated a wet snowcover by May 25th, which probably further explains the high backscatter of June 18th (-5.5 dB), when the snow most likely had melted away completely. By using the values in Table 4 one could also account for the backscatter differences of the lower and upper gully in the reference images. By January 9th (2005) and 23rd (2007) the lower gully backscattered -11.5 dB and -12 dB, whereas the backscatter values for the upper gully were -5.8 dB and -6.6 dB. According to the dB values in Table 4 would this demonstrate that the snowcover of the lower gully, in general, has higher water content than the upper part of the gully. This is actually possible seeing the diverse snow depths, as the lower gully is more hollow-shaped, and that the upper gully is more exposed to wind, which is a chilling factor.

The backscatter values of particular snowcovers presented in Table 4 are more applicable in the analysis of temporal backscatter variation than in the change detection analysis, due to different scales and value units. The change detection analysis rather has an emphasis on larger scale snowmelt, than on backscattering from one specific location as in the other analysis. Also, the results of the change detection analysis are presented as brightness changes in 8-bit digital values. A value of change is not equivalent to a value of backscattering. Instead of analyzing specific backscattering values, increased or decreased brightness is of interest, as we investigate which areas, or targets, that are objects of brightness change during the snowmelt season. As displayed in the Results chapter, the gully appears to be susceptible to snow wetness change.

## 7.4 The sensitivity of snow properties and SAR geometry on radar backscatter

The specific snow properties and the SAR geometry have a large impact on the radar backscatter, as already mentioned in this discussion. The sensitivity of volume- and surface backscatter are here plotted as functions of snow grain size, snow permittivity and incidence angle, to illustrate the effects on backscatter for each of them.

As shown by the surface scattering model in Eq. 1, surface scattering is for example, sensitive to the Fresnel reflection coefficient, which itself is a function of snow permittivity, and to the incidence angle of the satellite sensor. In Fig. 19, the functions of snow permittivity and incidence angle are shown. The model for volume scattering (see Eq. 3-4) is for example sensitive to the dielectric mixture model (K), which is itself a function of snow permittivity, and the radius of snow grains. The functions of snow permittivity and snow grain radius are shown in Fig. 20

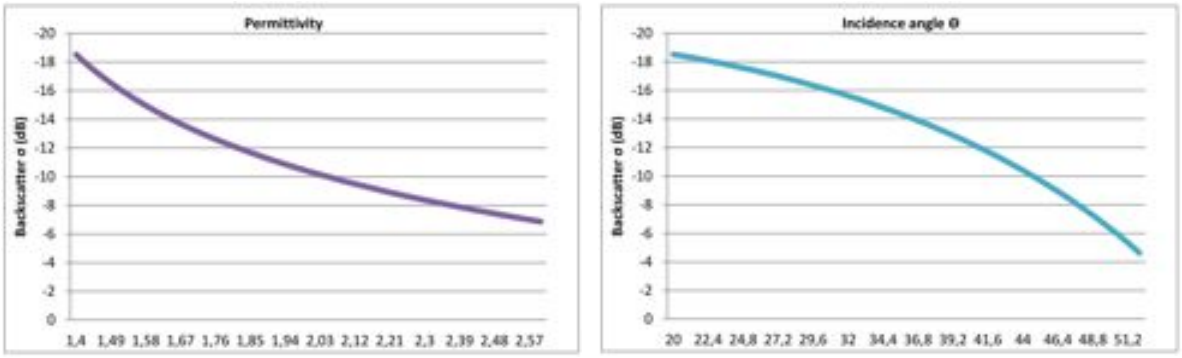


*Fig 17. (Left) The function of snow permittivity on the radar backscatter (dB), where snow permittivity is a part of the Fresnel reflection coefficient and (right) the function of incidence angle of the satellite sensor, for surface scattering*

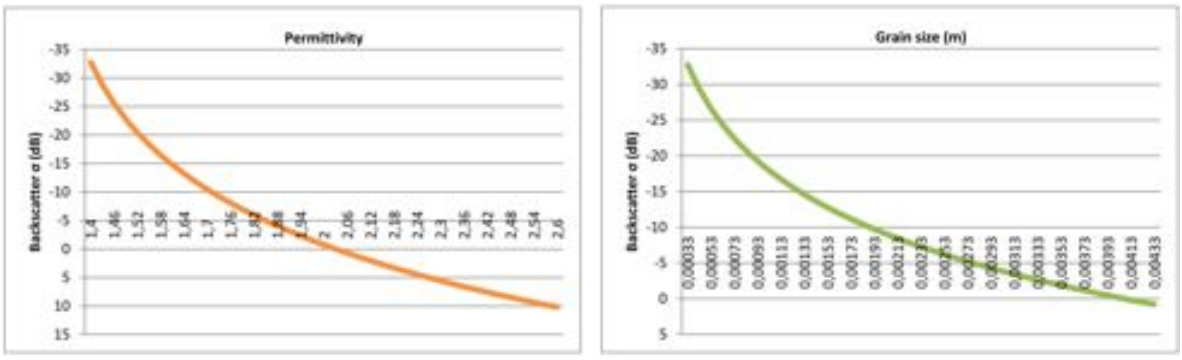


*Fig 18. (Left) The function of snow grain radius (m) on the radar backscatter (dB) and (right) the function of snow permittivity on the radar backscatter (dB), where snow permittivity is a part of the dielectric mixture model, for volume scattering*

If we compare the sensitivity of surface- and volume scattering to snow permittivity, we find that it has a larger impact on volume scattering than on surface scattering. When snow permittivity was changed from 1.4 to 2.6, it rose from -30 dB up to 10 dB for volume scattering, but only increased by 10 dB for surface scattering. In Fig. 17 we find that surface scattering is sensitive to the SAR geometry. By using the same snow properties and only

increasing the angle of incidence, we find that the backscatter increase dramatically, with 10 dB per 10° of incidence angle. By increasing the radius of the snow grain size, we find that for volume scattering, the backscatter increase with 5 dB per ~ 0.2 mm.

Evidently, snow properties and geometry cannot be compared to each other, but the plots show the sensitivity of the models to certain snow properties and geometry factors. When a parameter is used in both models, like the example of snow permittivity, a sensitivity analysis can be made. By doing so, we get an understanding for the complexity of these parameters depending on if we study a dry- or wet snowcover.

# 8. CONCLUSIONS

The geometric relationship between slope angle and incidence angle cannot be neglected in the mapping of snow. The impact of SAR geometry and snow properties on radar backscatter has in this study been emphasized, though the results indicated a snow wetness variation rather than a *direct* effect of SAR geometry. Two locations in the same gully can generate very different backscatter values due to their different level of altitude and specific slope angle in relation to the satellite sensor. For better accuracy when comparing backscatter values from snow surfaces at different locations, one requirement may therefore be to use locations of the same spatial characteristics and altitude so that the geometry to the sensor remains the same. It is extremely difficult to receive reliable backscatter values from an area of steep terrain. The spatial radar coverage over the central Brooks Range turns out to be poor due to wide-spread layover effects and shadowed areas. Some of the radiometric distortions could possibly have been avoided if the incidence angle was of a higher degree and if another digital elevation model had been used for terrain correction.

Snowpacks are dynamic and field measurements for each day of SAR acquisition are therefore desirable. If ground-truth data is lacking, parameters can be taken from the literature to be implemented in the surface- and volume scattering models, which in turn will generate backscatter values that are typical for each type of snowcover that is studied. However, there are parameters that are not included in the modeling but that are still important to include in such analyses, e.g. air temperature data. Air temperatures in 2007 were in accordance to the results of the temporal backscatter variation analysis. Air temperatures in 2005 also support the results of the analysis, but because of irregular measurements they are less consistent.

Slushflows and slush avalanches are too small in size to be seen in SAR imagery. Since the resolution of RADARSAT-1 FN1 mode is 6.25 m, backscatter from wet and dry snow, ice and even bare rock can be present within that area. These four medium backscatters differently which makes an average image, which is also processed with a speckle filter, not very representative for what might be present in the image in the reality.

With the SAR data available for this study and the long repeat cycle of the imagery used, it was not possible to catch any slush event in the year of 2005 and 2007. On the other hand, it may be possible to use SAR imagery to map wet snow areas on a larger scale and compare the wet snowcovers with topography. Modeling results of this paper showed that a backscatter value lower than -16 dB may be used as an indication for slush snow. Consequently, by interacting slush-prone locations with similar backscatter values, slushflow and slush avalanche risk zones can be monitored and used in annual snowmelt forecasting.

# ACKNOWLEDGEMENT

This study started as a class project at University of Alaska, Fairbanks, during spring 2011. I would like to show my greatest appreciation to Keith Cunningham and Matthias Braun for their help and support during that project. At Stockholm University, Sweden, the project developed into my bachelor thesis during the fall semester. I am deeply grateful to Ian Brown who has been my supervisor throughout the entire work and provided me with the best supervision one could get. Thanks to the close cooperation between University of Alaska and Stockholm University, I have had access to the SAR imagery monitored by the Alaska Satellite Facility.

Katreen Wikström

# REFERENCES


Alaska Mapped (2011) *Alaska* http://www.alaskamapped.org/data/arcgis-layer-files (Downloaded 04-28-11)

Baghdadi, N., Gauthier, Y., Bernier, M., Fortin, J. P. (2000) *Potential and limitations of RADARSAT SAR data for wet snow monitoring* IEEE Transactions on Geoscience and Remote Sensing, vol 38, no 1, January

Baghdadi, N., Livingstone, C. E., Bernier, M. (1998) *Airborne C-band SAR Measurements of Wet Snow-Covered Areas* IEEE Transactions on Geoscience and Remote Sensing, vol 36, no 6

Barber, D. G., LeDrew, E. F. (1994) *Modeling Synthetic Aperture Radar (SAR) scattering from a seasonally varying snow-covered sea ice volume at 5.3 and 9.25 GHz* Polar Research, vol 13, no 1, p. 35-54

Colbeck, S., Akitaya, E., Armstrong, R., Gubler, H., Lafeuille, J., Lied, K., McClung, D., Morris, E. (1990) The *International Classification for Seasonal Snow Cover on the Ground* The International Commission on Snow and Ice of the International Association of Scientific Hydrology

Colbeck, S. C. (1975) *Grain and bond growth in wet snow* Snow mechanics: Proceedings of a symposium held at Grindelwald, 1974, IAHS Publication, vol 114, p 51-61

Decaulne, A., Saemundsson, T. (2006) *Meteorological conditions during slush-flow release and their geomorpholocial impact in northwestern Iceland: A case study from the Bíldudalur valley* Swedish Society for Anthropology and Geography

Dean, A.M., Brown, I., Huntley, B., Thomas, C.J (2006) *Monitoring snowmelt across the Arctic forest-tundra ecotone using Synthetic Aperture Radar* International Journal of Remote Sensing, vol 27, no 19, p 4347-4370

Eckerstorfer, M., Christiansen, H. (2011) *Topographical and meteorological control on snow avalanching in Longyearbyen area, central Svalbard 2006-2009* Geomorphology, vol 134, p. 186-196

Eckerstorfer, M., Christiansen, H. (2010) *An extreme slush and slab avalanche event in high arctic maritime Svalbard* International Snow Science Workshop

ESA (2011a) *RADAR and SAR glossery* Earthnet Online, European Space Agency, Table 5.2 http://envisat.esa.int/handbooks/asar/CNTR5-2.htm (Downloaded 11-11-11)

ESA (2011b) *1.1.2 Scientific background* Earthnet Online, European Space Agency http://envisat.esa.int/handbooks/asar/CNTR1-1-2.htm (Downloaded 13-11-11)

Fily, M., Dedieu, J-P., Surdyk, S. (1995) *A SAR image study of a snow-covered area in the French Alps* Remote Sensing Environment, vol 51, p. 253-262

Guneriussen, T. (1997) *Backscattering properties of a wet snow cover derived from DEM corrected ERS-1 SAR data* International Journal of Remote Sensing, vol 18, no 2, p. 375-392

Hestnes, E., Sandersen, F. (2000) *The main principles of slushflow hazard mitigation* Internationales Symposium, Tagungspublikation, band 2, p. 267-280

Hestnes, E. (1998) *Slushflow hazard – where, why and when? 25 years of experience with slushflow consulting and research* Annals of Glaciology, vol 26

Jaedicke, C., Kern, M. A., Gauer, P., Baillifard, M. A., Platzer, K. (2008) *Chute experiments on slushflow dynamics* Cold Regions Science Technology, vol 51, p. 156-167

Koskinen, J. T., Pulliainen, J. T., Hallikainen, M. T. (1997) *The use of ERS-1 SAR data in snow melt monitoring* IEEE Transactions on Geoscience and Remote Sensing, vol 35, no 3

Martinez-Vazquez, A., Fortuny-Guasch, J., Gruder, U. (2005) *Monitoring of the snow cover with a ground-based synthetic aperture radar* EARSeL eProceedings, vol 4, no 1

Nagler, T., Rott, H. (2000) *Retrieval of wet snow by means of multitemporal SAR data* IEEE Transactions on Geoscience and Remote Sensing, vol 38, no 2

Nature Resource Conservation Service (2011) Atigun Pass. Air temperatures 2005 and 2007-2011 http://www.wcc.nrcs.usda.gov/nwcc/site?sitenum=957&state=ak (Downloaded 11-25-11)

Nyberg, R., Rapp, A. (1998) *Extreme erosional events and natural hazards in Scandinavian mountains* Ambio, vol 27, no 4

O'harra, D. (2001) *Atigun Pass avalanche control article* Anchorage Daily News, published 2001-02-26

Onesti, L. J. (1987) *Slushflow release mechanism: A first approximation* Avalanche Formation, Movement and Effects, no 162

Onesti, L. J. (1985) Meteorological *conditions that initiate slushflows in the central Brooks Range, Alaska* Annals of Glaciology, vol 6

Partington, K. C. (1998) *Discrimination of glacier facies using multi-temporal SAR data* Journal of Glaciology, vol 44, no 146

RADARSAT (2008) *RADARSAT Data Products Specifications* RS1-GS-026, D4

Rees, W. G. (2001) *Physical principles of remote sensing* Second Edition, Cambridge University Press

Rott, H. and Nagler, T. (1993) *Snow and glacier investigations by ERS-1 SAR – first results* Rep. ERA SP-359, European Space Agency, Paris, p. 577-582

Sharma, S. S., Mathur, P., Snehmani (2004) *Change detection analysis of avalanche snow in Himalayan region using near infrared and active microwave images* Advances in Space Research, vol 33, p. 259-267

Shi, J., Dozier, J. (1995) *Inferring snow wetness using C-band data from SIR-C's polarimetric Synthetic*

*Aperture Radar* IEEE Transactions on Geoscience and Remote Sensing, vol 33, no 4

Singh, G. and Venkataraman, G. (2010) *Snow permittivity retrieval inversion algorithm for estimating snow wetness* Geocarto International, vol 25, no 3, p. 187-212

Strozzi, T., Wegmüller, U., Mätzler, C. (1999) *Mapping wet snowcovers with SAR interferometry* International Journal of Remote Sensing, vol 20, no 12, p 2395-2403

Tremper, B. (2008) *Staying alive in avalanche terrain* Mountaineers Books

Ulaby, F. T., Moore, R. K., Fung, A. K. (1982) *Microwave remote sensing Vol 2 – Radar remote sensing and surface scattering and emission theory,* Addison-Wesley, Advanced Book Program, Reading, Massachusetts

Walker, M.D., Walker, D.A., Welker, J.M., Arft, A.M., Bardsley, T., Brooks, P.D., Fahnestock, J.T., Jones, M.G., Loslebehn, M., Parsons, A.N., Seastedt, T.R., Turner., P.l. (1999) *Long-term experimental manipulation of winter snow regime and summer temperature in arctic and alpine tundra.* Hydrological Processes, vol 17, p 2315-2330

Xiao, J., Li, J., Moody, A. (2003) *A detail-preserving and flexible adaptive filter for speckle suppression in SAR imagery* International Journal of Remote Sensing, vol 24, no 12, p. 2451-2465

# ATTACHED DOCUMENTS

## 1. 8-bit RGB greyscale values converted to decibel values

| | | | |
|---|---|---|---|
| 52 -48,252071 | 99 -35,548535 | 146 -22,844999 | 193 -10,141463 |
| 53 -47,981783 | 100 -35,278247 | 147 -22,574711 | 194 -9,871175 |
| 54 -47,711495 | 101 -35,007959 | 148 -22,304423 | 195 -9,600887 |
| 55 -47,441207 | 102 -34,737671 | 149 -22,034135 | 196 -9,330599 |
| 56 -47,170919 | 103 -34,467383 | 150 -21,763847 | 197 -9,060311 |
| 57 -46,900631 | 104 -34,197095 | 151 -21,493559 | 198 -8,790023 |
| 58 -46,630343 | 105 -33,926807 | 152 -21,223271 | 199 -8,519735 |
| 59 -46,360055 | 106 -33,656519 | 153 -20,952983 | 200 -8,249447 |
| 60 -46,089767 | 107 -33,386231 | 154 -20,682695 | 201 -7,979159 |
| 61 -45,819479 | 108 -33,115943 | 155 -20,412407 | 202 -7,708871 |
| 62 -45,549191 | 109 -32,845655 | 156 -20,142119 | 203 -7,438583 |
| 63 -45,278903 | 110 -32,575367 | 157 -19,871831 | 204 -7,168295 |
| 64 -45,008615 | 111 -32,305079 | 158 -19,601543 | 205 -6,898007 |
| 65 -44,738327 | 112 -32,034791 | 159 -19,331255 | 206 -6,627719 |
| 66 -44,468039 | 113 -31,764503 | 160 -19,060967 | 207 -6,357431 |
| 67 -44,197751 | 114 -31,494215 | 161 -18,790679 | 208 -6,087143 |
| 68 -43,927463 | 115 -31,223927 | 162 -18,520391 | 209 -5,816855 |
| 69 -43,657175 | 116 -30,953639 | 163 -18,250103 | 210 -5,546567 |
| 70 -43,386887 | 117 -30,683351 | 164 -17,979815 | 211 -5,276279 |
| 71 -43,116599 | 118 -30,413063 | 165 -17,709527 | 212 -5,005991 |
| 72 -42,846311 | 119 -30,142775 | 166 -17,439239 | 213 -4,735703 |
| 73 -42,576023 | 120 -29,872487 | 167 -17,168951 | 214 -4,465415 |
| 74 -42,305735 | 121 -29,602199 | 168 -16,898663 | 215 -4,195127 |
| 75 -42,035447 | 122 -29,331911 | 169 -16,628375 | 216 -3,924839 |
| 76 -41,765159 | 123 -29,061623 | 170 -16,358087 | 217 -3,654551 |
| 77 -41,494871 | 124 -28,791335 | 171 -16,087799 | 218 -3,384263 |
| 78 -41,224583 | 125 -28,521047 | 172 -15,817511 | 219 -3,113975 |
| 79 -40,954295 | 126 -28,250759 | 173 -15,547223 | 220 -2,843687 |
| 80 -40,684007 | 127 -27,980471 | 174 -15,276935 | 221 -2,573399 |
| 81 -40,413719 | 128 -27,710183 | 175 -15,006647 | 222 -2,303111 |
| 82 -40,143431 | 129 -27,439895 | 176 -14,736359 | 223 -2,032823 |
| 83 -39,873143 | 130 -27,169607 | 177 -14,466071 | 224 -1,762535 |
| 84 -39,602855 | 131 -26,899319 | 178 -14,195783 | 225 -1,492247 |
| 85 -39,332567 | 132 -26,629031 | 179 -13,925495 | 226 -1,221959 |
| 86 -39,062279 | 133 -26,358743 | 180 -13,655207 | 227 -0,951671 |
| 87 -38,791991 | 134 -26,088455 | 181 -13,384919 | 228 -0,681383 |
| 88 -38,521703 | 135 -25,818167 | 182 -13,114631 | 229 -0,411095 |
| 89 -38,251415 | 136 -25,547879 | 183 -12,844343 | 230 -0,140807 |
| 90 -37,981127 | 137 -25,277591 | 184 -12,574055 | 231 0,129481 |
| 91 -37,710839 | 138 -25,007303 | 185 -12,303767 | 232 0,399769 |
| 92 -37,440551 | 139 -24,737015 | 186 -12,033479 | 233 0,670057 |
| 93 -37,170263 | 140 -24,466727 | 187 -11,763191 | 234 0,940345 |
| 94 -36,899975 | 141 -24,196439 | 188 -11,492903 | 235 1,210633 |
| 95 -36,629687 | 142 -23,926151 | 189 -11,222615 | 236 1,480921 |
| 96 -36,359399 | 143 -23,655863 | 190 -10,952327 | 237 1,751209 |
| 97 -36,089111 | 144 -23,385575 | 191 -10,682039 | 238 2,021497 |
| 98 -35,818823 | 145 -23,115287 | 192 -10,411751 | 239 2,291785 |